ADVANCED FUNCTIONAL MATERIALS
www.afm-journal.de

Wet Chemistry Vitrification and Metal-to-Semiconductor Transition of 2D Gray Arsenene Nanoflakes

Yi Hu, Xinzhu Wang, Zhenghang Qi, Susu Wan, Junchuan Liang, Qingqing Jia, Daocheng Hong, Yuxi Tian, Jing Ma, Zuoxiu Tie, and Zhong Jin**

To manipulate the electrical and optical properties of 2D materials via engineering their phases and crystallinity is of great significance for the construction of nanodevices with versatile functions. Herein, the controllable transformation of semimetallic gray arsenene nanoflakes into semiconducting vitreous arsenene nanoflakes via a wet chemistry vitrification method is reported. Experimental studies and theoretical simulations reveal that the vitrification of gray arsenene nanoflakes is attributed to the consumption of arsenic atoms by aqueous HF via the trigger of dissolved oxygen, resulting in a significant variation of band structure rendered by the formation of atomic structure disorderliness and arsenic atom defects/vacancies. Unlike the semimetallic features of pristine gray arsenene nanoflakes, the as-prepared vitreous arsenene nanoflakes exhibit a strong photoluminescence peak centered at 635 nm corresponding to an optical band gap of 1.95 eV, and the field-effect transistors based on vitreous arsenene nanoflakes also exhibit definitely *p*-type semiconducting characteristics with a carrier mobility of ≈159.1 $cm^2 V^{-1} s^{-1}$. The wet chemistry induced vitrification of gray arsenene nanoflakes presents an efficient strategy to regulate the electrical and optical properties of arsenene nanoflakes, providing new insights for the interface and band structure engineering of 2D nanomaterials.

1. Introduction

2D materials have drawn intense attention in the past decade due to their fantastic properties and potential applications in nanoelectronic devices.[1–5] The quantum confinement effect of 2D materials brings exotic physical and chemical properties, such as distinct anisotropies, bandgaps, carrier mobilities, and optoelectronic properties, which are very different from the features of corresponding bulk materials. Thus, 2D materials have exhibited significant potential in field-effect transistors (FETs), photodetectors, light-emitting diodes (LEDs), solar cells, and flexible and wearable devices, holding great promise to change the future configurations of semiconductor architectures.[6–10] Among the representative 2D materials, group-VA analogues of graphene, such as phosphorene, arsenene, antimonene, and bismuthene, are of increasing interest due to their intriguing electronic properties and promising applications.[11–15] Arsenene, as a member of group-VA 2D materials, has three allotropes, including gray arsenene (rhombohedral), black arsenene (orthorhombic), and yellow arsenene (As_4 molecular crystal).[11,12,16] The different crystalline phases lead to distinct electrical properties. Few-layer gray arsenene with a buckled honeycomb structure is semimetallic, while mono- and few-layer black arsenene with a crystal structure similar to black phosphorus depicts semiconductor feature, and yellow arsenene is insulating.[11,12,17] Theoretical simulations have predicted that gray arsenene shall exhibit an emerging bandgap when its thickness is reduced to bilayers or monolayer.[14,18–20] Although few-layer arsenene nanoflakes have been prepared by liquid-phase exfoliation,[21–23] the semimetallic feature and ambient oxidation hinder the applications in optoelectronics and FET devices. So far, it is still a great challenge to obtain monolayer or bilayer arsenene, let alone effective preservation in ambient air. Our group has developed a van der Waals epitaxy method for achieving high-crystallinity few-layer gray arsenene nanoflakes and proposed a universal approach to greatly improve the ambient stability of arsenene nanoflakes via polymer passivation,[24] paving the way for the subsequent modification, processing, and nanodevice applications. To further manipulate the physical and chemical properties of arsenene, it is of key importance to develop rational ways to precisely regulate its atomic configuration and electrical structure and meanwhile preserve the special 2D morphology. From this perspective, converting the semimetallic gray arsenene into semiconductor would be an effective way to facilitate the applications of gray arsenene in nanoelectronics and optoelectronics.

Herein, we report the conversion of semimetallic gray arsenene nanoflakes into semiconductive vitreous arsenene

Y. Hu, X. Wang, Z. Qi, S. Wan, J. Liang, Q. Jia, D. Hong, Y. Tian, J. Ma, Z. Tie, Z. Jin
MOE Key Laboratory of Mesoscopic Chemistry
MOE Key Laboratory of High Performance Polymer Materials and Technology
Jiangsu Key Laboratory of Advanced Organic Materials
School of Chemistry and Chemical Engineering
Nanjing University
Nanjing 210023, China
E-mail: majing@nju.edu.cn; zhongjin@nju.edu.cn
Y. Hu, J. Liang, Z. Tie, Z. Jin
Shenzhen Research Institute of Nanjing University
Shenzhen 518063, China
The ORCID identification number(s) for the author(s) of this article can be found under https://doi.org/10.1002/adfm.202106529.

DOI: 10.1002/adfm.202106529

nanoflakes through wet chemistry treatment of aqueous hydrofluoric acid (HF) solution. The arsenene nanoflakes can be controllably vitrified starting from one side or both sides and be transferred to arbitrary substrates with the assistance of polymer coating. Detailed structural characterizations confirm the typical vitrification characteristics of vitreous arsenene nanoflakes, which are obviously distinguished from the high-crystallinity pristine gray arsenene nanoflakes. The as-prepared vitreous arsenene nanoflakes show a broad and strong photoluminescence (PL) emission peak centered at a wavelength of 635 nm, corresponding to an optical band gap of 1.95 eV. Moreover, FET devices based on vitreous arsenene nanoflakes show a typical gate-controlled on/off effect and a carrier mobility of ≈159.1 cm^2 V^{-1} s^{-1}. By combining experimental studies and theoretical simulations, we find that the vitrification of gray arsenene nanoflakes shall be attributed to the surface etching and random consumption of As atoms triggered by dissolved oxygen during the immersion in aqueous HF solution.

2. Results and Discussions

The gray arsenene nanoflakes with a tunable thickness range of 4–48 nm were grown on mica substrates via a van der Waals epitaxy method, as detailed in the Methods Section. **Figure 1**a illustrates typical optical photograph and Raman spectrum of a freshly prepared few-layer gray arsenene nanoflake, exhibiting a regular hexagonal shape with a diagonal length of ≈10 µm. The inserted Raman spectrum shows two Raman peaks with frequencies of 195.3 and 254.5 cm^{-1}, which are consistent with the E_g (second-order in-plane vibration) and A_{1g} (first-order out-of-plane vibration) modes of gray arsenic, respectively.[25] The vitrification of gray arsenene nanoflakes was achieved via an aqueous HF solution treatment process, which can be conducted with or without the protection of the polymer film on the upper surface (Figure 1b–e).

The vitrification process that started from one side (lower surface) was realized with the assistance of polymethyl methacrylate (PMMA) coating on the upper surface and then immersed into the aqueous HF solution (Figure 1b,c). During this process, the upper surface of nanoflakes was initially protected, and the vitrification began from the lower surface attached on mica substrate and infiltrated by HF. By adjusting the duration of HF treatment, the gray arsenene nanoflakes could be partially (Figure 1b) or completely vitrified (Figure 1c). After transferred on a SiO_2/Si substrate, the optical photographs showed that both the partially vitrified

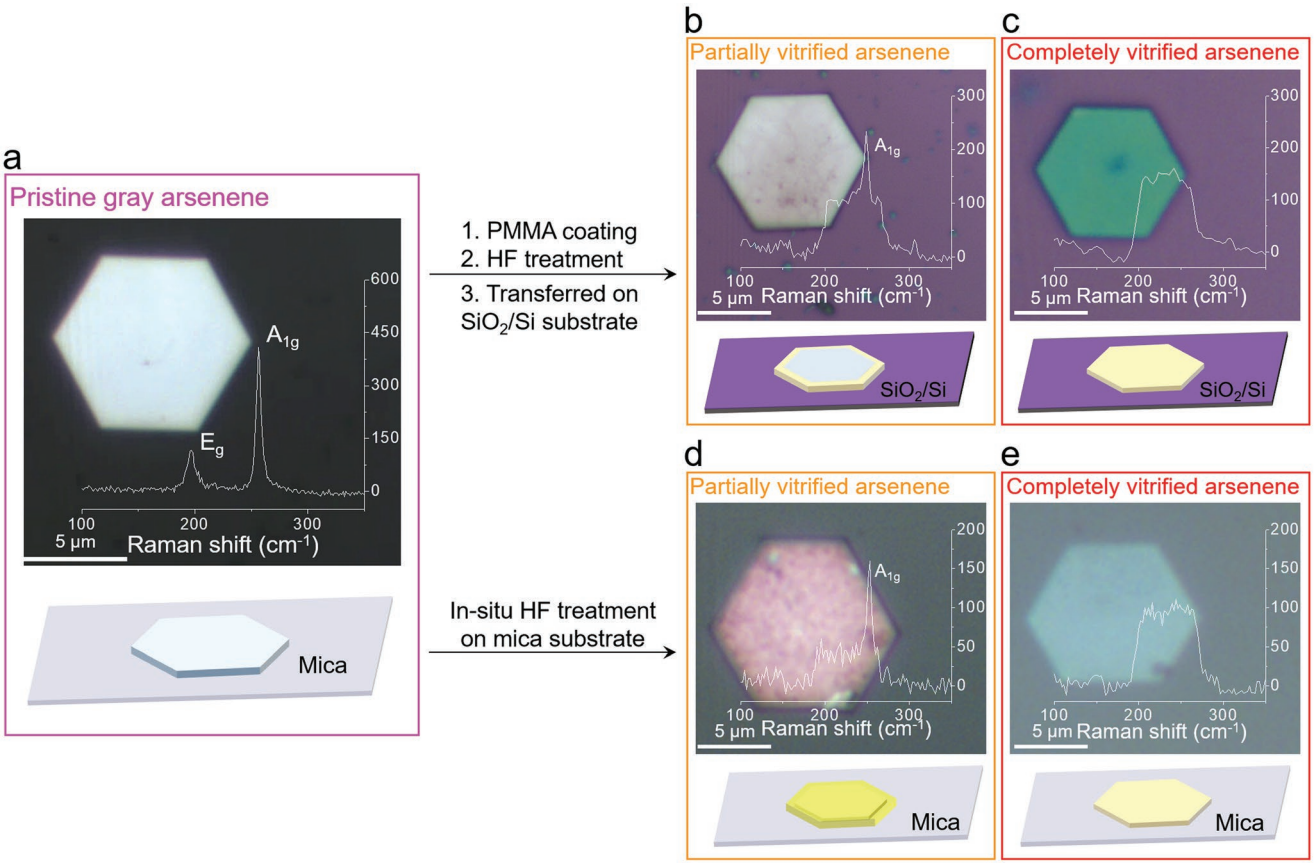

Figure 1. The vitrification of gray arsenene nanoflakes via wet chemistry treatment. a) Optical photograph and schematic diagram of a pristine gray arsenene nanoflake grown on mica substrate; the inset illustrates the corresponding Raman spectrum. b,c) Optical photographs, Raman spectra, and schematic diagrams of b) partially, and c) completely vitrified arsenene nanoflakes yielded after polymer coating, subsequent HF treatment and then transferred onto SiO_2/Si substrate. d,e) Optical photographs, Raman spectra, and schematic diagrams of d) partially and e) completely vitrified arsenene nanoflakes on mica substrate achieved by in situ immersion in aqueous HF solution.

and completely vitrified arsenene nanoflakes well maintained their initial hexagonal shape (the insets of Figure 1b,c), while the Raman spectra were obviously changed in comparison with pristine gray arsenene nanoflakes. The Raman spectrum of partially vitrified arsenene nanoflakes showed a sharp peak centered at 248 cm^{-1} (A_{1g} peak) and a broad band range from 200 to 260 cm^{-1}, in accordance with the Raman features of gray and amorphous arsenic species, respectively.[25,26] Notably, no Raman signals of arsenic oxides or other impurities were detected, indicating that the vitrification process made no variation on the chemical composition of arsenene nanoflakes. The surface color of partially vitrified arsenene nanoflakes was similar to that of freshly synthesized gray arsenene nanoflakes, suggesting that the upper surface was well protected by the PMMA film and the vitrification mainly proceeded from the lower surface. By prolonging the duration of HF treatment, the A_{1g} peak of gray arsenene was completely changed to the broad band of vitreous arsenene (Figure 1c), and the surface color totally converted into green, indicating that the entire nanoflake was completely transformed into vitrified arsenene nanoflake. Moreover, to investigate the protection effect of different polymers, polyacrylonitrile (PAN) was also used to protect the upper surface of arsenene nanoflakes. As illustrated in Figure S1, Supporting Information, the optical microscopy images and Raman spectra of the partially and completely vitrified arsenene nanoflakes protected by PAN show identical results with those of PMMA protected arsenene nanoflakes, indicating that some other polymers can also protect the upper surface of arsenene nanoflakes and assist in the transfer of arsenene nanoflakes to other substrates. In the polymer protected vitrification method, the polymer films play a key role of surface protection and transfer medium. Thus, inert polymers, that do not react with arsenene and HF or dissolve in water, can be reasonably employed as protecting polymers. Moreover, the removability is also important for choosing suitable protecting polymers. Moreover, the concentrations of PMMA solutions mainly affect the quality, uniformity, and thickness of PMMA films. We found that the PMMA solution with a low concentration of 1 wt% is difficult in forming continuous PMMA films, while a high PMMA concentration of 10 wt% reduces the flexibility of PMMA films and hinders the high-quality transfer of arsenene nanoflakes.

As an alternative, the vitrification process could also be in situ conducted by directly immersing the mica substrate into HF solution, and the vitrification began simultaneously from the both sides of nanoflakes in this case, since the mica surface is susceptible to HF infiltration (Figure 1d,e). The Raman spectra of the in situ vitrified arsenene nanoflakes have identical Raman features compared to the PMMA-protected samples. However, the upper surface color of in situ partially vitrified arsenene nanoflake (Figure 1d) was obviously different from those of the freshly prepared gray arsenene nanoflake (Figure 1a) and PMMA-protected sample (Figure 1b), confirming that the upper surface without polymer protection directly underwent the vitrification. Due to the different colors and contrasts of Si/SiO_2 and mica substrates, the completely vitrified arsenene nanoflakes on mica substrate show light blue color, which is different from the green color on Si/SiO_2 substrate (Figure 1c,e).

To investigate the optimized parameters for in situ wet chemistry vitrification of gray arsenene nanoflakes on mica substrates, the etching of arsenene nanoflakes using different concentrations of HF solutions and under different vitrification periods were performed, as illustrated in Figure S2, Supporting Information. Higher HF concentration normally results in higher vitrification degree of arsenene nanoflakes at the same etching duration. Besides, when etched with same concentration of HF solution, the vitrification degree of arsenene nanoflakes are gradually increased over time. The HF solution with lower concentration (1 wt%) will takes more time to achieve completely vitrified arsenene nanoflakes, while the higher concentration of HF solution (10 wt%) will leads to rapid vitrification of arsenene nanoflakes and increase the difficulty in controlling the vitrification of arsenene nanoflakes. Thus, 5 wt% HF aqueous solution is applicable in controllable vitrification of arsenene nanoflakes, in which 30 and 50 min etching is suitable for obtaining partially and completely vitrified arsenene nanoflakes.

The partially and completely vitrified arsenene nanoflakes were transferred onto Cu grids to study the crystalline structure variations. **Figure 2**a illustrates a typical transition electron microscopy (TEM) image of a completely vitrified arsenene nanoflake, which well preserves its original hexagonal morphology. However, the atomic configuration of completely vitrified arsenene nanoflakes (Figure 2b,c) is thoroughly amorphous, which is totally distinct from that of pristine gray arsenene nanoflakes, indicating that the vitrification process has induced significant change of atomic structure, resulting in disordered atomic arrangement. High-resolution TEM (HRTEM) image (Figure 2c) and corresponding select area electron diffraction (SAED) pattern (the inset of Figure 2c) of completely vitrified arsenene nanoflake confirm its vitreous characteristics. To further understand the evolution of crystallinity during the vitrification process, TEM images and SAED patterns were collected from different positions of a partially vitrified arsenene nanoflake, as shown in Figure 2d–h. The low-magnification TEM image (Figure 2d) shows two distinct regions with different contrasts, indicating the boundary of vitrified and almost unvitrified parts. The HRTEM and SAED images collected from the middle region (pink square) show highly crystalline feature (Figure 2e,f), preserving the high crystal quality of pristine gray arsenene nanoflake. In contrast, the SEAD pattern collected from the edge region (blue square) depicts a typical vitreous character (Figure 2g). Notably, the SEAD pattern measured at the boundary region (yellow square) showed both crystalline and vitreous features (Figure 2h), indicating the distinguishing crystalline features between the vitrified and unvitrified parts.

To intuitively observe the vitrification process, optical microscopy images of arsenene nanoflakes with different vitrification degrees on Si/SiO_2 substrate were collected, as shown in Figure S3, Supporting Information. The blue and white areas are well identified as the vitreous arsenene phase and gray arsenene phase by Raman spectra, respectively (Figure S3e–f, Supporting Information). Thus, it proves that the edge region of arsenene nanoflake is more reactive and tends to be more rapidly vitrified than the middle region. These results reveal that the vitrification starts from the edge part that directly

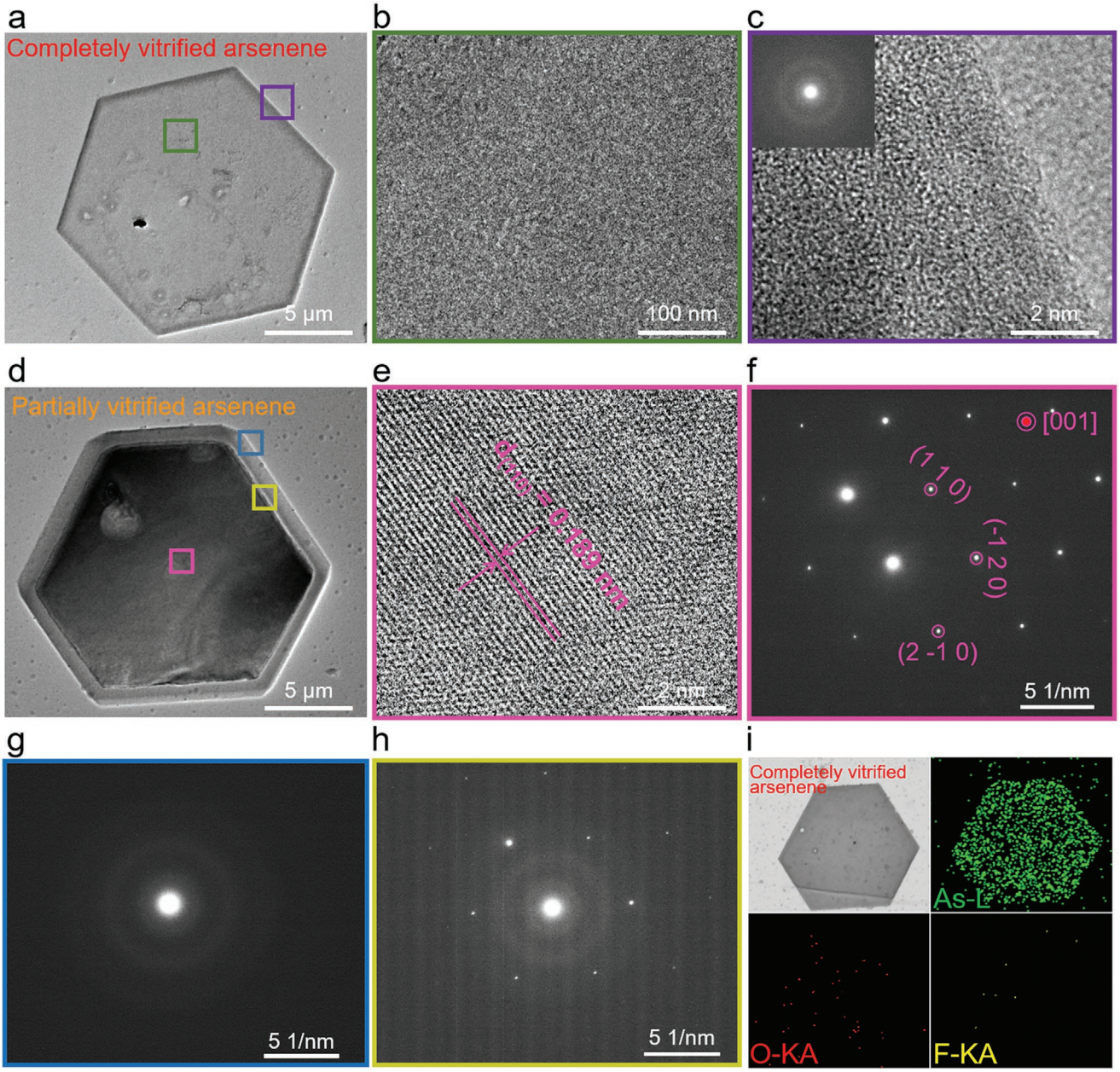

Figure 2. Structure and composition characterizations. a) TEM image of a completely vitrified arsenene nanoflake. b) Magnified TEM image collected from the region of green square in (a). c) HRTEM image and corresponding SEAD pattern collected from the region of purple square in (a). d) Low-magnified TEM image of a partially vitrified arsenene nanoflake. e) HRTEM image collected from the region of pink square in (d). f–h) SAED patterns collected from the regions of f) pink, g) blue, and h) yellow squares in (d). i) TEM image and corresponding elemental mapping images of a completely vitrified arsenene nanoflake.

interacted with aqueous HF solution, and then slowly extends to the interior part, confirming the gradual vitrification process of arsenene nanoflake. The vitrification starting from the edge parts should be attributed to the earliest contact with HF and the abundant dangling bonds at edge parts. The edge parts with dangling bonds are more reactive and thus have lower reaction energy barriers to HF solution and dissolved oxygen than the interior parts. Moreover, the continuous extending of vitreous arsenene from the edge to the interior part also demonstrate that the vacancy defects formed by oxidation and HF attack serve as the reaction frontier and lead the vitrification of gray arsenene (Figure S3b–d, Supporting Information).

To investigate the composition evolution induced by wet chemistry vitrification, TEM and corresponding element mapping images (Figure 2i) of a completely vitrified arsenene nanoflake were collected, revealing a homogeneous spatial distribution of As element and negligible amounts of O and F. Moreover, energy dispersive X-ray spectra of pristine gray arsenene nanoflake and completely vitrified arsenene nanoflake show similar content of As and trace amounts of O and F elements

(Figure S4a,b, Supporting Information). The O content of completely vitrified arsenene nanoflake is much less than another control sample of surface-oxidized gray arsenene nanoflake prepared by exposing in ambient air for 175 min (Figure S4c, Supporting Information), confirming the HF treatment leads to crystalline vitrification rather that surface oxidation. X-ray photoelectron spectroscopy (XPS) analysis of pristine gray arsenene nanoflakes illustrates a narrow band with two sharp peaks corresponding to As $3d_{3/2}$ and As $3d_{5/2}$ (Figure S5a, Supporting Information), which are consistent with gray arsenic crystal.[24] In contrast, the As 3d band of completely vitrified arsenene nanoflakes is much broader (Figure S5b, Supporting Information), indicating the more complex chemical environment and high disorderliness of As atoms. Notably, the XPS spectrum of surface-oxidized gray arsenene nanoflakes gives a new peak of As_2O_3 (Figure S5c, Supporting Information) and its TEM images show obviously polyporous characteristics (Figure S6, Supporting Information), which is distinctly different from completely vitrified arsenene nanoflakes (Figure S5b, Supporting Information, and Figure 2a). These results suggest that the elemental arsenic composition of arsenene nanoflakes after the vitrification process is well preserved, instead of being converted to arsenic oxides.

Micro-Raman mapping was performed to distinctly identify the gray arsenic phase and vitreous arsenic phase in vitrified arsenene nanoflakes. As shown in the inset of Figure 1, when the vitrification degree of arsenene nanoflake increase, the peak intensity of A_{1g} band at the wavenumber of 254 cm^{-1} correspondingly decreases and the broad band at 225 cm^{-1} increases. Hence, we can use the A_{1g} band intensity mapping at 254 cm^{-1} to recognize crystalline gray arsenic phase and the Raman intensity mapping at 225 cm^{-1} to discern vitreous arsenic phase. The optical photographs and micro-Raman mapping profiles of a pristine gray arsenene nanoflake, a partially vitrified arsenene nanoflake and a completely vitrified arsenene nanoflake were compared in **Figure 3**a–i. The intensity mapping at 254 cm^{-1} (A_{1g} peak intensity mapping) of pristine gray arsenene nanoflake shows uniform distribution of Raman signals and almost identical response area corresponding to its optical microscopy image, confirming its high homogeneity (Figure 3a,b). Besides, the Raman intensity mapping at 225 cm^{-1} depicts just background signals (Figure 3c), indicating that the pristine gray arsenene nanoflake has no vitreous arsenic phase.

For partially vitrified arsenene nanoflake prepared with PMMA protection (Figure 3d), the Raman mapping at 254 cm^{-1} (Figure 3e) shows uniform distribution of strong Raman signals at the middle region but much lower Raman signals at the edge region, indicating that the edge of this nanoflake has been fully vitrified because the edge parts with dangling bonds have higher reactivity compared to middle region during the vitrification process, which is consistent with the TEM image in Figure 2d. Conversely, the Raman intensity mapping at 225 cm^{-1} (Figure 3f) shows an identical response area compared to its optical microscopy image (Figure 3d), but the Raman signals at the middle region are weak and the signals at the edge region are much stronger. This result also suggests that vitrification degree at the edge region is much higher than that of the middle region protected by PMMA coating, because HF first contacts and penetrates into the edge region of the nanoflake. It confirms that the vitrification on the edge and surface of arsenene nanoflakes take precedence over that in the interior. In contrast, for the completely vitrified arsenene nanoflake, both the Raman intensity mappings at 254 and 225 cm^{-1} illustrate almost the same homogeneous signal distributions (Figure 3g–i). Moreover, the Raman signal intensities at 254 and 225 cm^{-1} are almost identical, confirming the complete transition of the entire arsenene nanoflake from gray arsenic phase to vitreous arsenic phase.

PL spectroscopy analysis was performed to investigate the optical properties of pristine and vitreous arsenene nanoflakes (Figure 3j–l). Pristine gray arsenene nanoflakes exhibit almost no PL response, owing to the semimetallic characteristic with continuous energy band levels and zero band gap (Figure 3j). In contrast, the PL spectrum of completely vitrified arsenene nanoflakes present a broad and strong emission peak centered at 635 nm when excited by a 473 nm laser, corresponding to an optical band gap of 1.95 eV. For comparison, the PL spectrum of commercial A_2O_3 powders was also collected, giving a very weak emission peak centered at 553 nm. The emission peak position of As_2O_3 is obviously different from that of completely vitrified arsenene nanoflakes, verifying that the PL signal of completely vitrified arsenene nanoflakes originates from the semiconductive vitreous arsenic phase rather than the surface oxidation. Previous PL studies on few layer MoS_2 demonstrated that the intensity of PL spectra (I_{Lum}) can directly reflect the PL quantum efficiency (η_{Lum}) after normalizing with Raman intensity (I_{Raman}), which can be presented as the formula: $\eta_{Lum} = \eta_{Raman}(I_{Lum}/I_{Raman})$.[27] Thus, the Raman intensity of gray arsenene and vitreous arsenene nanoflakes in PL spectra are normalized and illustrated in Figure 3j. It is evident that the luminescence quantum efficiency of arsenene nanoflakes is greatly increased after vitrification, confirming the PL emission enhancement of vitreous arsenene nanoflakes. The strong PL intensity should be attributed to the As defects/vacancies caused by HF vitrification that act as the recombination center of holes and electrons. Moreover, the vitrified arsenene nanoflakes is a typical 2D nanomaterial with large surface area and strong quantum confinement effect (Figure 2c and **Figure 5**b), which can also potentially increase the PL intensity.

The PL features, including imaging, stability, and lifetime, of vitrified arsenene nanoflakes were then detailedly investigated by using a 450 nm laser as the excitation source. The PL image of two partially vitrified arsenene nanoflakes shows luminescence only at the edge regions (the top inset of Figure 3k), suggesting that the occurrence of vitrification mainly at the edge regions, which is in accordance with the TEM characterization (Figure 2d) and Raman mappings (Figure 3e,f). In contrast, the PL image of two completely vitrified arsenene nanoflakes exhibits strong luminescence over the entire areas with clearly hexagonal shapes (the bottom inset of Figure 3k), indicating the homogeneous and thorough vitrification of the entire nanoflakes. The PL intensity profile as a function of time collected from the red spot in the bottom inset of Figure 3k shows only slight fluctuations within 1 min, demonstrating the high luminescence stability of the completely vitrified arsenene nanoflakes. The radiative recombination process of excitons was subsequently studied via PL decay lifetime analysis. As illustrated in Figure 3l, the decay lifetime curve of completely

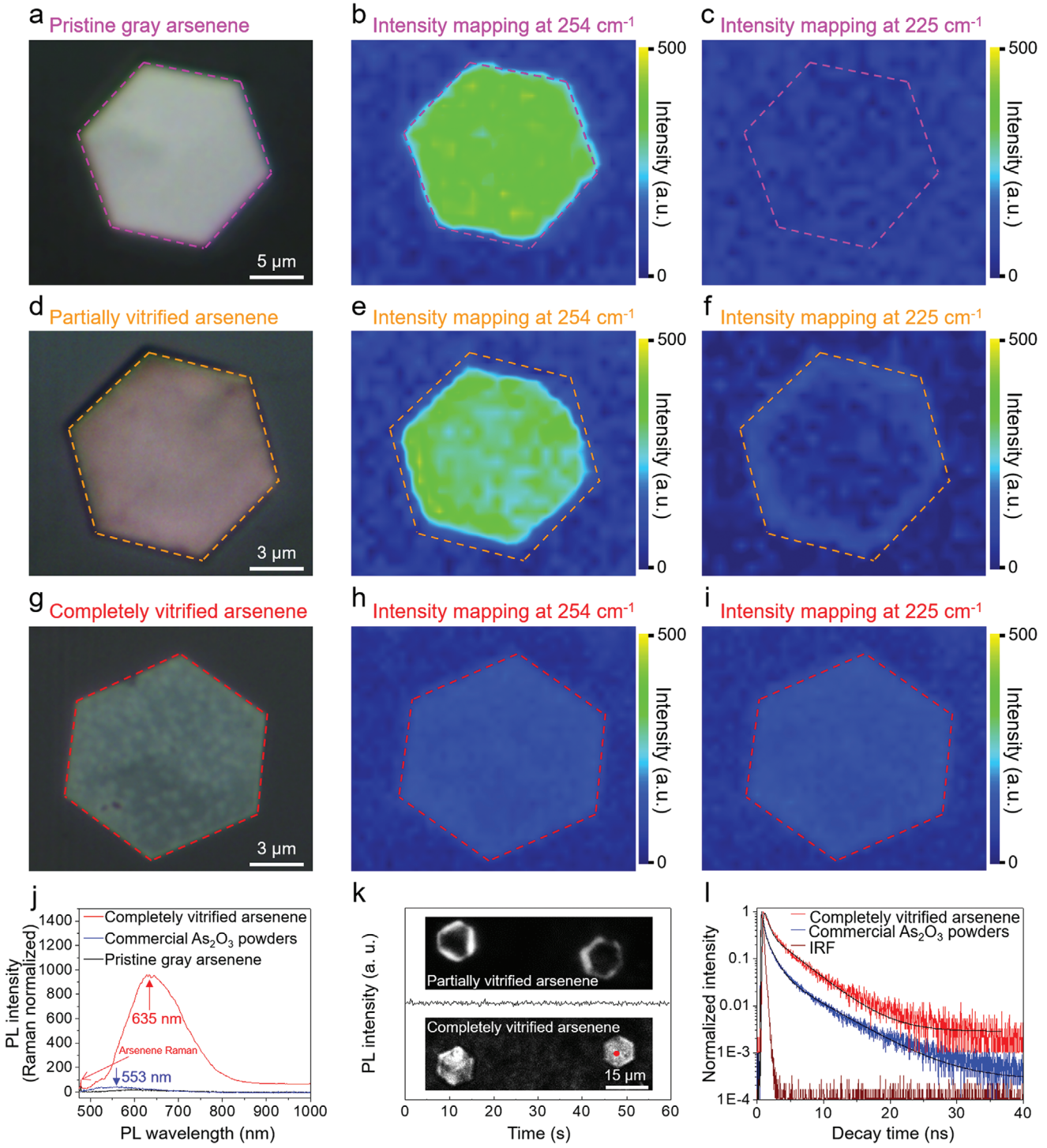

Figure 3. Spectral characterizations. a,d,g) Optical photographs, b,e,h) Raman intensity mappings at 254 cm^{-1}, and c,f,i) Raman intensity mappings at 225 cm^{-1} of a–c) a pristine gray arsenene nanoflake, d–f) a partially vitrified arsenene nanoflake, and g–i) a completely vitrified nanoflake, respectively. j) Intensity-normalized PL spectra of pristine gray arsenene nanoflakes (black line), completely vitrified arsenene nanoflakes (red line), and commercial As_2O_3 powders (blue line). k) PL stability of a completely vitrified arsenene nanoflake (measured at the position of red dot in the bottom inset). The insets in (k) show the PL photographs of (top) two partially vitrified and (bottom) two completely vitrified arsenene nanoflakes. l) PL decay lifetime curves of completely vitrified arsenene (red line) and commercial As_2O_3 powders (blue line). The instrumental response function is also included for reference.

vitrified arsenene nanoflakes is fitted with a triexponential function, demonstrating a carrier lifetime of 2.9 ns. In contrast, commercial A_2O_3 powders exhibits a carrier lifetime of 1.2 ns, further confirming that the PL signal of as-prepared vitreous arsenene nanoflakes are not originated from ambient oxidation. The intriguing PL properties of vitreous arsenene nanoflakes

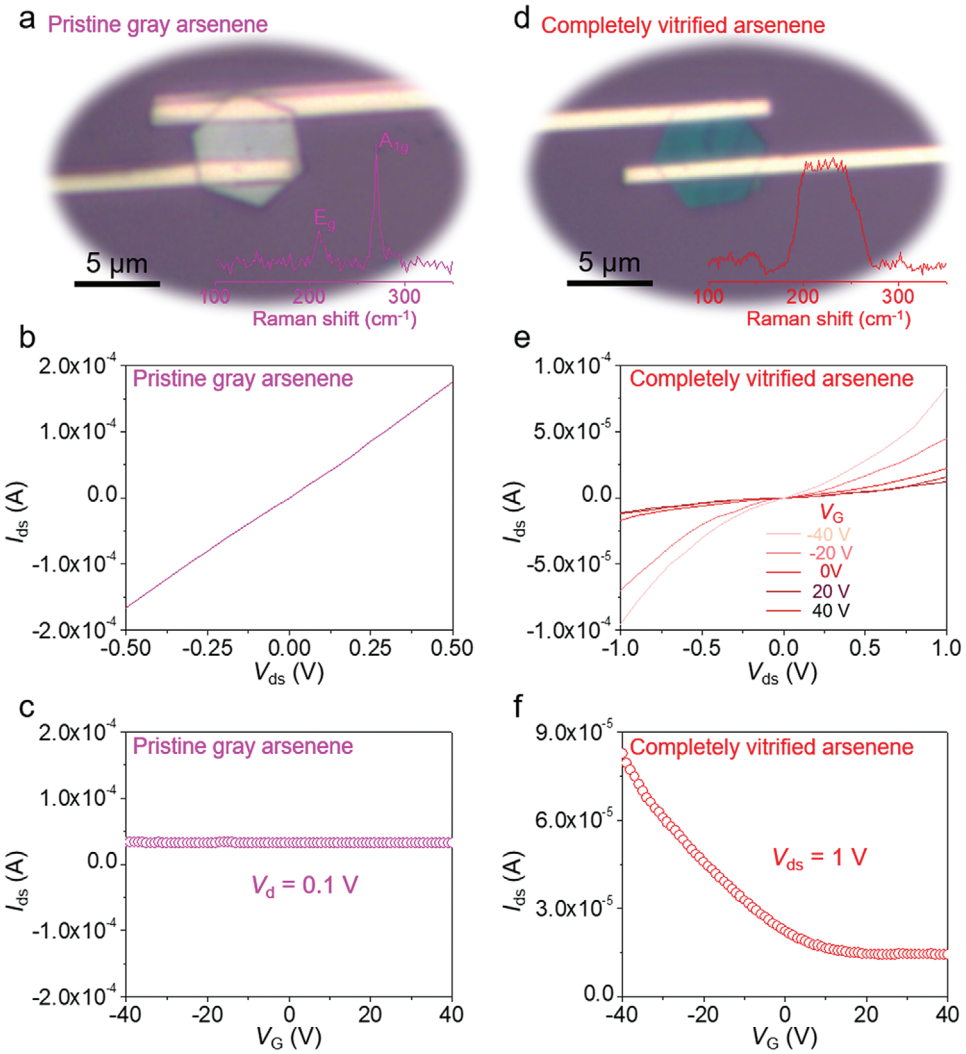

Figure 4. Measurements of carrier transport properties. a–f) Optical photographs and corresponding Raman spectra (a,d), *I–V* curves (b,e), and corresponding transfer characteristics curves (c,f) of two-terminal devices based on a pristine gray arsenene nanoflake (a–c) and a completely vitrified arsenene nanoflake (b–f).

imply a broad prospect for the applications in the fields of photonics and optoelectronics.

To explore the carrier transport properties of gray arsenene nanoflakes before and after vitrification process, two-terminal devices based on pristine gray arsenene nanoflakes and completely vitrified arsenene nanoflakes were fabricated on SiO_2/Si substrates, as detailed in the Methods Section. **Figure 4**a illustrates a typical two-terminal device based on a pristine gray arsenene nanoflake with a thickness of 30 nm. The channel length and width of the device are 2.5 and 6 μm, respectively. The gray arsenene nanoflake maintains its pristine metal luster after the transfer and device fabrication. The crystalline phase was also confirmed by Raman spectroscopy (the inset of Figure 4a), indicating that the nanoflake transfer and device fabrication steps make no effect on the crystal quality of gray arsenene nanoflake. The *I–V* curve of pristine gray arsenene nanoflake based device suggests Ohmic contact (Figure 4b), and the corresponding transfer characteristic curve demonstrates constant drain current during the gate voltage sweep from −40 to 40 V (Figure 4c). The electrical conductivity was calculated with the equation: $\sigma = I_d L / V_d W t$, where I_d is the drain current, V_d is the drain voltage, L, W, and t is the channel length, channel width, and thickness of gray arsenene, respectively. The calculated electrical conductivity is $\approx 5.1 \times 10^3$ S m^{-1}, confirming the well-maintained semimetallic features and relatively high electrical conductivity of pristine gray arsenene. In contrast, the optical photograph of completely vitrified arsenene nanoflake shows a prominently green color, and the corresponding Raman spectrum confirms its vitreous feature (Figure 4d). The output and transfer curves of completely vitrified arsenene nanoflake based FET device show typical *p*-type semiconducting characteristics (Figure 4e,f). The contact between completely vitrified arsenene nanoflake and Au electrodes shows a typical Schottky behavior (Figure 4e), indicating that the vitrification process changes the work function of arsenene nanoflake. The drain current of completely vitrified arsenene nanoflake-based

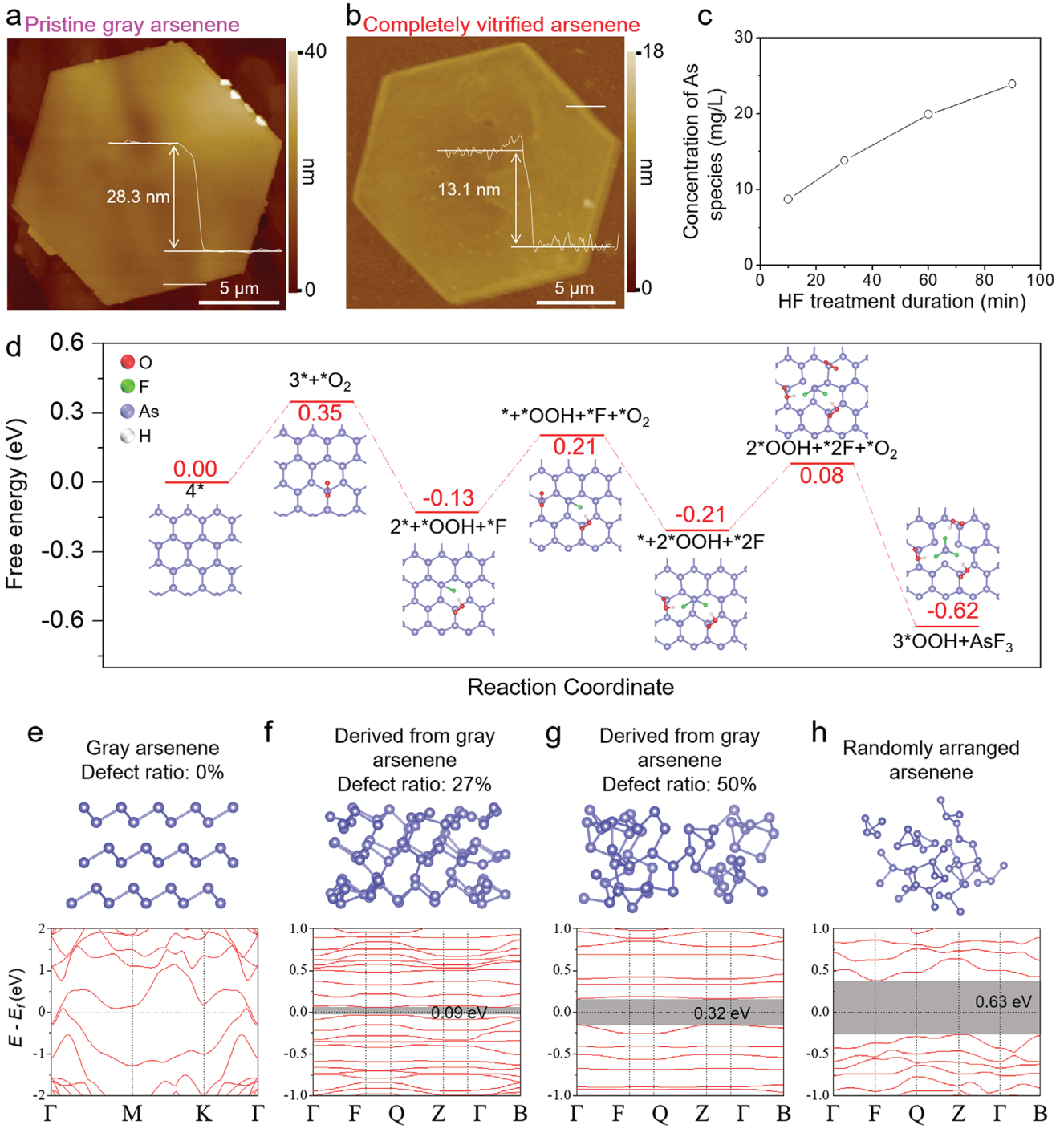

Figure 5. Mechanism studies of the vitrification process. a,b) AFM images and corresponding height profiles of a) a pristine gray arsenene nanoflake and b) after the complete vitrification process. c) The concentration of As species after different duration of immersion in aqueous HF solution measured by dual-channel atomic fluorescence spectrometer. d) DFT-calculated free energy profile and corresponding intermediate structures of the proposed vitrification reaction pathway. e–h) Simulated atomic structures and corresponding electronic band structures derived from three-layer gray arsenene models with different defect ratios of e) 0%, f) 27%, g) 50%, and h) a randomly arranged vitreous arsenene model. The Fermi level (gray short dashed lines) of each system is set to 0 eV.

FET device (Figure 4e,f) obviously reduces when the gate bias increases from –40 V to 40 V, exhibiting a *p*-type carrier transport behavior and an on/off ratio of ≈5.6. The carrier mobility of completely vitrified arsenene nanoflake can be calculated with the equation: $\mu = (dI_{ds}/dV_g) \times (L/WC_iV_{ds})$, where $L = 2.5$ μm is the channel length, $W = 6$ μm is the channel width, V_{ds} is the drain-source bias, and $C_i = 11.5 \times 10^{-5}$ F m^{-1} is the capacitance of 300-nm-thick SiO_2 dielectric layer. Thus, the

carrier mobility is calculated to be ≈159.1 $cm^2\ V^{-1}\ s^{-1}$ at room temperature, which is of the same order of magnitude as the carrier mobility achieved in MoS_2, black phosphorus, and tellurene.[28–30] The high carrier mobility shall be attributed to that some buckled honeycomb atom structures of gray arsenene phase are remained after vitrification, thus resulting in the high drain currents of vitreous arsenene FET at a drain voltage of 1 V and the high calculated carrier mobility. These results further confirm the metal-to-semiconductor transition of gray arsenene nanoflakes via wet chemistry vitrification, which provide an effective approach to broaden the nanoelectronics and photoelectronics applications of arsenene materials.

To further understand the mechanism of vitrification process, the morphology and thickness variations of arsenene nanoflakes before and after aqueous HF treatment were investigated by atomic force microscopy (AFM). The AFM image of a typical gray arsenene nanoflake depicts a smooth and flat surface topography (Figure 5a), while the surface becomes relatively rough after the complete vitrification process (Figure 5b). This phenomenon should be ascribed to the etching of HF solution, resulting in the irregular arrange of As atoms on the surface of vitrified arsenene. Moreover, the etching of arsenene nanoflakes also induced the thickness decrease of the nanoflakes. Moreover, the concentration of As species dissolved in aqueous HF solution measured via a dual-channel atomic fluorescence spectrometer (Figure 5c) is obviously increased as the treatment duration prolongs, indicating that the arsenene nanoflakes is slowly etched by aqueous HF solution. To study the role of ambient air atmosphere in the vitrification process, control experiments were performed by treating gray arsenene nanoflakes in aqueous HF solution under continuous N_2 protection (Figure S7, Supporting Information). Notably, the vitrification rate of gray arsenene nanoflakes under continuous N_2 protection (Figure S7, Supporting Information) is significantly slower than that exposed in ambient air with identical concentration of HF (Figure S2b, Supporting Information). Even after immersed in aqueous HF solution under continuous N_2 protection for 100 min, the Raman signals of arsenene nanoflake were almost unchanged, with only a slight enhancement of the broad band of vitreous arsenic phase between 200–260 cm^{-1} (Figure S7, Supporting Information). In contrast, the arsenene nanoflake treated in aqueous HF solution under ambient air exposure underwent rapid vitrification in 10 min, and finally completely vitrified after 50 min (Figure S2b, Supporting Information). These control experiments suggest that the dissolved oxygen in aqueous HF solution can significantly promote the vitrification of arsenene nanoflakes, forming As defects/vacancies and unsaturated As atoms that facilitates the transition of gray arsenene into vitreous arsenene. Electron paramagnetic resonance (EPR) spectra were also measured to identify the potential defects/vacancies of pristine gray arsenene nanoflakes. As shown in Figure S8, Supporting Information, the EPR spectrum of gray arsenene nanoflakes shows similar signals to the background, indicating that the freshly prepared arsenene nanoflakes have negligible lattice defects.

Based on the above experimental findings, the possible chemical reaction route for the wet chemistry vitrification of gray arsenene nanoflakes in aqueous HF solution can be described as follows:

$$4As + 3O_2 \rightarrow 2As_2O_3 \quad (1)$$

$$As_2O_3 + 6HF \rightarrow 2AsF_3 + 3H_2O \quad (2)$$

$$\text{Overall: } 2As + 6HF + O_2 \rightarrow 2AsF_3 + 3H_2O \quad (3)$$

It is known that pure arsenic crystals can react with oxidizing acids but not with nonoxidizing acids.[31] In our case, the O_2 molecules may play an important role in the wet chemistry vitrification process, and the direct vitrification of gray arsenene nanoflakes by HF without O_2 exposure is unfeasible, possibly due to the high reaction energy barrier. The dissolved oxygen in aqueous HF solution may result in trace oxidation on the surface of gray arsenene nanoflakes (Equation (1)). Then, the formed arsenic oxides can react with HF, generating AsF_3 that is easily hydrolyzed and leading to the vitrification of arsenene nanoflakes (Equation (2)). Hence, a possible reaction pathway was theoretically proposed to show how oxygen molecules promote the reaction between gray arsenene and HF (Figure 5d). In the initial step, O_2 molecules dissolved in the HF solution arrive at the surface of the arsenene and then attach to As atom sites. Then, the H^+ ions cooperated with the adsorbed oxygen in HF solution to form an *OOH intermediate, and the F^- ions are bonded with the neighboring As atoms on the arsenene surface. One arsenic vacancy and one AsF_3 molecule are obtained after three cycles. The free energy difference of the first step is ≈0.35 eV, which could be easily realized at room temperature. After each cycle, the energy costs of oxygen attack and F^- ions bond become lower, indicating that the defects potentially promote the further oxygen attack and F^- bonding and also likely to act as the reaction frontier. These results suggest that the As vacancies and edge defects in gray arsenene nanoflakes generated from oxidation and HF attack may play an important role in promoting the further vitrification of arsenene nanoflakes. Many As defects are introduced into the arsenene nanoflakes as the reaction continually occurred, generating a large number of unsaturated As atoms in the arsenene. Furthermore, density functional theory (DFT) calculations also demonstrate that the unsaturated As atoms tended to interact/bond with the adjacent unsaturated As atoms, breaking the long-range order of the arsenic crystal and rearranging the As atoms.

The vitrification of gray arsenene nanoflakes results to As defects and crystal structure disorderliness, which are supposed to be the key factors affecting the electronic band structures. Thus, to evaluate the electronic band structure of arsenene nanoflakes after vitrification, two different DFT simulation strategies were designed to construct the models of vitreous arsenene, respectively focusing on the effects of As defects/vacancies and structural disorderliness on the electrical structure of vitreous arsenene. The first model preserved partial gray arsenene structure and highlights the influence of As defects/vacancies on the band structure of arsenene, while the later model emphasized the disorderliness of arsenene structure.

The first one was achieved by manually constructing random As defects in the atomic structure of three-layer gray arsenene ($4 \times 4 \times 1$ supercell), and then implemented a further structural optimization. Figure 5e–g illustrate the typical atomic structures (upon) and corresponding band structures (below) of arsenene with the defect ratios of 0%, 27%, and 50%, respectively. The pristine three-layer gray arsenene with 0% defect ratio shows typical semimetallic feature without band gap (Figure 5e). In contrast, the arsenene with random As defects/vacancies and structure optimization show apparent band gaps (Figure 5f,g). With the defect ratio increases from 27 to 50% (fewer As atoms left in atomic structures), the band gap accordingly enlarges from 0.09 to 0.32 eV, indicating that the defects and structural deformations caused by atomic As defects/vacancies can effectively open the band gap.

To further enhance the disorderliness of arsenene, another atomic model with completely disordered arrangement of arsenic atoms was also constructed (Figure 5h). In contrast, the band structure of randomly arranged vitreous arsenene with a $3 \times 3 \times 1$ supercell depicts a band gap of 0.63 eV, which is much wider than the band gap of vitreous arsenene model derived from gray arsenene (0.32 eV, Figure 5g).

The experimentally measured optical band gap is ≈1.95 eV, which is much larger than the calculated band gaps of DFT-simulated vitreous arsenene models derived from defective gray arsenene (0.32 eV) or randomly arranged arsenene (0.63 eV). This is because due to the calculation speed limitation of computer system, only arsenene models with supercells of $3 \times 3 \times 1$ and $4 \times 4 \times 1$ are established. Moreover, not all of physical parameters can be considered in the modeling, such as the density change, the reduced thickness and the interaction with the substrate. Thus, the theoretically predicted band gaps are different from the experimentally measured band gap to some extents. However, the theoretical stimulations are still remarkable in revealing the influences of As defects and structure disorderliness on the band structure of arsenene. These results suggest that the vitrification process of arsenene nanoflakes generates As defects and crystal structure disorderliness, breaking the regular arrangement and continuous connection of arsenic atoms and changing the energy band structure. Moreover, the DFT-calculated band structures of vitreous arsenene reveal that some energy levels disappeared or changed due to the introduction of As defects and crystal structure disorderliness. These band structure changes lead to the band gap opening of vitreous arsenene nanoflakes and also results in the enhanced PL emission (Figure 3j). It also indicates that the wet chemistry vitrification of arsenene nanoflakes by aqueous HF solution is an effective way to regulate the electrical properties of arsenene nanoflakes.

3. Conclusion

In summary, we demonstrate that semimetallic gray arsenene nanoflakes can be transformed into semiconducting vitreous arsenene nanoflakes through a wet chemistry vitrification process in aqueous HF solution. The obtained vitreous arsenene nanoflakes maintain identical shapes but thinner thickness and significant atomic structure disorderliness compared to pristine gray arsenene nanoflakes with high crystallinity. The as-prepared vitreous arsenene nanoflakes exhibit strong PL emission centered at a wavelength of 635 nm, which is distinct from the pristine semimetallic gray arsenene nanoflakes. Moreover, the FET devices based on completely vitrified arsenene nanoflakes show a prominent *p*-type semiconducting feature and a considerable carrier mobility of ≈159.1 $cm^2 V^{-1} s^{-1}$. By combining experimental investigations and theoretical calculations, we suggest that the vitrification of gray arsenene nanoflakes shall be attributed to the atomic As defects/vacancies-induced crystal structure reconstruction triggered by dissolved oxygen and surface oxidation during the treatment in aqueous HF solution. The wet chemistry vitrification is demonstrated as an effective way to manipulate the electrical and optical properties of arsenene nanoflakes, broadening its applications in electronics and photonics.

Supporting Information

Supporting Information is available from the Wiley Online Library or from the author.

Acknowledgements

This work was financially supported by the National Key Research and Development Program of China (2017YFA0208200), the Fundamental Research Funds for the Central Universities of China (0205-14380266), the Natural Science Foundation of China (22022505, 21872069), the Natural Science Foundation of Jiangsu Province (BK20180008), and the Shenzhen Fundamental Research Program of Science, Technology and Innovation Commission of Shenzhen Municipality (JCYJ20180307155007589). The authors are also grateful to the High Performance Computing Center (HPCC) of Nanjing University for carrying out numerical calculations on its blade cluster system.

Conflict of Interest

The authors declare no conflict of interest.

Author Contributions

Z.J. and Y.H. conceived the idea of this manuscript and designed the experiments. Y.H. performed the synthesis, Raman characterizations, and data analysis. J.C.L. and Z.X.T. performed the AFM and TEM characterizations. S.S.W., D.C.H., and Y.X.T. performed the photoluminescence analysis. X.Z.W., Z.H.Q., Q.Q.J., and J.M. did the theoretical simulations and calculations. All the authors analyzed the data and discussed the results. Y.H. and Z.J. co-wrote and revised the manuscript. Z.J. and J.M. supervised the project.

Data Availability Statement

Research data are not shared.

Keywords

2D materials, arsenic nanoflakes, vitrification arsenene, wet chemistry vitrification

Received: July 7, 2021
Revised: August 29, 2021
Published online:

[1] K. S. Novoselov, A. K. Geim, S. V. Morozov, D. Jiang, Y. Zhang, S. V. Dubonos, I. V. Grigorieva, A. A. Firsov, *Science* **2004**, *306*, 666.
[2] Q. H. Wang, K. Kalantar-Zadeh, A. Kis, J. N. Coleman, M. S. Strano, *Nat. Nanotechnol.* **2012**, *7*, 699.
[3] J. S. Ross, P. Klement, A. M. Jones, N. J. Ghimire, J. Q. Yan, D. G. Mandrus, T. Taniguchi, K. Watanabe, K. Kitamura, W. Yao, D. H. Cobden, X. D. Xu, *Nat. Nanotechnol.* **2014**, *9*, 268.
[4] L. K. Li, Y. J. Yu, G. J. Ye, Q. Q. Ge, X. D. Ou, H. Wu, D. L. Feng, X. H. Chen, Y. B. Zhang, *Nat. Nanotechnol.* **2014**, *9*, 372.
[5] D. Voiry, H. Yamaguchi, J. W. Li, R. Silva, D. C. B. Alves, T. Fujita, M. W. Chen, T. Asefa, V. B. Shenoy, G. Eda, M. Chhowalla, *Nat. Mater.* **2013**, *12*, 850.
[6] S. Das, R. Gulotty, A. V. Sumant, A. Roelofs, *Nano Lett.* **2014**, *14*, 2861.
[7] F. Wang, Z. X. Wang, L. Yin, R. Q. Cheng, J. J. Wang, Y. Wen, T. A. Shifa, F. M. Wang, Y. Zhang, X. Y. Zhan, J. He, *Chem. Soc. Rev.* **2018**, *47*, 6296.
[8] M. L. Tsai, S. H. Su, J. K. Chang, D. S. Tsai, C. H. Chen, C. I. Wu, L. J. Li, L. J. Chen, J. H. He, *ACS Nano* **2014**, *8*, 8317.
[9] S. Z. Butler, S. M. Hollen, L. Y. Cao, Y. Cui, J. A. Gupta, H. R. Gutierrez, T. F. Heinz, S. S. Hong, J. X. Huang, A. F. Ismach, E. Johnston-Halperin, M. Kuno, V. V. Plashnitsa, R. D. Robinson, R. S. Ruoff, S. Salahuddin, J. Shan, L. Shi, M. G. Spencer, M. Terrones, W. Windl, J. E. Goldberger, *ACS Nano* **2013**, *7*, 2898.
[10] D. Lembke, S. Bertolazzi, A. Kis, *Acc. Chem. Res.* **2015**, *48*, 100.
[11] M. Pumera, Z. Sofer, *Adv. Mater.* **2017**, *29*, 1605299.
[12] S. L. Zhang, S. Y. Guo, Z. F. Chen, Y. L. Wang, H. J. Gao, J. Gomez-Herrero, P. Ares, F. Zamora, Z. Zhu, H. B. Zeng, *Chem. Soc. Rev.* **2018**, *47*, 982.
[13] X. Wang, J. Song, J. L. Qu, *Angew. Chem., Int. Ed.* **2019**, *58*, 1574.
[14] G. Pizzi, M. Gibertini, E. Dib, N. Marzari, G. Iannaccone, G. Fiori, *Nat. Commun.* **2016**, *7*, 12585.
[15] S. L. Zhang, M. Q. Xie, F. Y. Li, Z. Yan, Y. F. Li, E. J. Kan, W. Liu, Z. F. Chen, H. B. Zeng, *Angew. Chem., Int. Ed.* **2016**, *55*, 1666.
[16] *Chemistry of Arsenic, Antimony and Bismuth*, (Ed. N. C. Norman), Springer, New York **1998**.
[17] G. N. Greaves, S. R. Elliott, E. A. Davis, *Adv. Phys.* **1979**, *28*, 49.
[18] Y. Y. Wang, P. Huang, M. Ye, R. Quhe, Y. Y. Pan, H. Zhang, H. X. Zhong, J. J. Shi, J. Lu, *Chem. Mater.* **2017**, *29*, 2191.
[19] S. L. Zhang, Z. Yan, Y. F. Li, Z. F. Chen, H. B. Zeng, *Angew. Chem., Int. Ed.* **2015**, *54*, 3112.
[20] C. Kamal, M. Ezawa, *Phys. Rev. B* **2015**, *91*, 085423.
[21] R. Gusmao, Z. Sofer, D. Bousa, M. Pumera, *Angew. Chem., Int. Ed.* **2017**, *56*, 14417.
[22] X. Wang, Y. Hu, J. Mo, J. Zhang, Z. Wang, W. Wei, H. Li, Y. Xu, J. Ma, J. Zhao, Z. Jin, Z. Guo, *Angew. Chem., Int. Ed.* **2020**, *59*, 5151.
[23] Z. H. Qi, Y. Hu, Z. Jin, J. Ma, *Phys. Chem. Chem. Phys.* **2019**, *21*, 12087.
[24] Y. Hu, Z. H. Qi, J. Y. Lu, R. P. Chen, M. Z. Zou, T. Chen, W. J. Zhang, Y. R. Wang, X. L. Xue, J. Ma, Z. Jin, *Chem. Mater.* **2019**, *31*, 4524.
[25] J. S. Lannin, J. M. Calleja, M. Cardona, *Phys. Rev. B* **1975**, *12*, 585.
[26] J. S. Lannin, *Phys. Rev. B* **1977**, *15*, 3863.
[27] A. Splendiani, L. Sun, Y. B. Zhang, T. S. Li, J. Kim, C. Y. Chim, G. Galli, F. Wang, *Nano Lett.* **2010**, *10*, 1271.
[28] B. Radisavljevic, A. Radenovic, J. Brivio, V. Giacometti, A. Kis, *Nat. Nanotechnol.* **2011**, *6*, 147.
[29] Y. X. Wang, G. Qiu, R. X. Wang, S. Y. Huang, Q. X. Wang, Y. Y. Liu, Y. C. Du, W. A. Goddard, M. J. Kim, X. F. Xu, P. D. Ye, W. Z. Wu, *Nat. Electron.* **2018**, *1*, 228.
[30] M. Buscema, D. J. Groenendijk, S. I. Blanter, G. A. Steele, H. S. J. van der Zant, A. Castellanos-Gomez, *Nano Lett.* **2014**, *14*, 3347.
[31] P. Patnaik, *Handbook of Inorganic Chemicals*, McGraw-Hill, New York **2003**, p. 529.